AIAA JOURNAL
Vol. 32, No. 7, July 1994

Direct Simulation Monte Carlo and Navier-Stokes Simulations of Blunt Body Wake Flows

James N. Moss* and Robert A. Mitcheltree†
NASA Langley Research Center, Hampton, Virginia 23681
Virendra K. Dogra‡
ViGYAN, Inc., Hampton, Virginia 23666
and
Richard G. Wilmoth‡
NASA Langley Research Center, Hampton, Virginia 23681

Numerical results obtained with direct simulation Monte Carlo and Navier-Stokes methods are presented for a Mach-20 nitrogen flow about a 70-deg blunted cone. The flow conditions simulated are those that can be obtained in existing low-density hypersonic wind tunnels. Three sets of flow conditions are considered with freestream Knudsen numbers ranging from 0.03 to 0.001. The focus is on the wake structure: how the wake structure changes as a function of rarefaction, what the afterbody levels of heating are, and to what limits the continuum models are realistic as rarefaction in the wake is progressively increased. Calculations are made with and without an afterbody sting. Results for the afterbody sting are emphasized in anticipation of an experimental study for the current flow conditions and model configuration. The Navier-Stokes calculations were made with and without slip boundary conditions. Comparisons of the results obtained with the two simulation methodologies are made for both flowfield structure and surface quantities.

Nomenclature

A = base area of cone, $\pi d^2/4$
C_D = drag coefficient, $2D/\rho_\infty V_\infty^2 A$
C_H = heat transfer coefficient, $2q/\rho_\infty V_\infty^3$
D = drag
d = base diameter
Kn = Knudsen number, λ/d
M = Mach number
$\bar{M}$ = molecular weight of N_2, 28.02 g/mole
R = gas constant for N_2, 296.7 J/kg-K
R_b = cone base radius
R_c = corner radius
Re = Reynolds number, $\rho V d/\mu$
Re_2 = total Reynolds number, Re_∞ (μ_∞/μ_0)
R_n = nose radius
S = speed ratio, $V\sqrt{\bar{M}/2RT}$
s = distance along the body surface measured from the stagnation point
$\bar{s}$ = temperature exponent of the coefficient of viscosity
T = thermodynamic temperature
T_i = internal kinetic temperature
T_{ov} = overall kinetic temperature
T_w = surface temperature
u = axial velocity
V = velocity
v = radial velocity
x = axial distance from stagnation point measured along symmetry axis
x_b = location of model base plane
x_s = location of wake stagnation point
y = radial distance from symmetry axis
Γ = gamma function
γ = ratio of specific heats, $\gamma = 1.4$
Δ = size of vortex, $(x_s - x_b)$
λ = mean free path
μ = dynamic viscosity
ρ = density
σ = collision cross section

Subscripts

ref = reference value
w = surface values
∞ = freestream values

Introduction

DETERMINATION of wake closure is a critical issue for aerobrakes because the low lift-to-drag ratio aeroshell designs impose constraints on payload configuration/spacecraft design. The issue is that the payload should fit into the wake in such a manner as to avoid the shear layer impingement to minimize heating. A perception exists[1] that the aerothermodynamics of wake flows cannot be accurately predicted. This perception occurs because two complicating phenomena can coexist for aerobraking application. One phenomena is caused by rarefaction effects that occur as the relatively high-density forebody flow expands into the wake. At typical perigees,[2] local Knudsen numbers of the order of 0.1 occur in the near wake. Consequently, continuum analyses become inadequate for describing near wake conditions encountered at substantially higher altitudes. The second phenomena, due to high aerobrake velocities, is the influence of thermochemical nonequilibrium on the wake structure as highly dissociated flow expands into the wake. The combination of these two phenomena brings into question the applicability of several aspects of physical models implemented in current computational tools, aspects that have limited testing against experimental data.

Presented as Paper 93-2807 at the AIAA 28th Thermophysics Conference, Orlando, FL, July 6-9, 1993; received Aug. 31, 1993; revision received Feb. 7, 1994; accepted for publication Feb. 17, 1994.

*Research Engineer, MS 366. Fellow AIAA.
†Research Engineer, MS 366. Member AIAA.
‡Research Engineer, MS 366. Senior Member AIAA.

Two different approaches are readily available for simulating wake flows under low-density conditions. One is the continuum approach in which a set of model equations is solved numerically. Normally, this set of equations is the Navier-Stokes equations. These equations can be extracted from the Boltzmann equation by retaining terms up to first order using the Chapman-Enskog expansion. Because the expansion parameter is essentially a local Knudsen number, the Navier-Stokes modeling becomes deficient for flows exhibiting large local Knudsen numbers. The second approach is a molecular approach where in a direct physical simulation is achieved by following the motion and interaction of modeled molecules. In the present study, computational codes representative of both approaches are used to simulate hypersonic wake flows about a 70-deg blunted cone. The continuum simulations are achieved with the Langley aerothermodynamics upwind relaxation algorithm (LAURA) of Gnoffo et al.[2,3] and Gnoffo[4] whereas the molecular simulations are achieved with Bird's[5-7] direct simulation Monte Carlo (DSMC) method. Both LAURA[2] and DSMC[8-10] have been used to examine the wake structure behind aerobrakes. References 10–14 are examples of recent applications of the DSMC method to blunt body wake studies. In these studies, the same flow conditions have not been calculated with both methods. Consequently, the present study focuses on applications of LAURA and DSMC for identical flow conditions. The conditions selected for simulation are attainable in low-density wind tunnels.[15] Consequently, the importance of chemical reactions on wake structure is not addressed in the present study.

The objectives of the current study are twofold: provide an improved understanding of the effects of rarefaction on blunt body wake structure and clarify the boundaries for realistic application of the Navier-Stokes algorithms with respect to rarefaction effects. Calculations are made using both DSMC and Navier-Stokes for the blunted cone both with and without a sting. In addition, the Navier-Stokes calculations were made with and without slip boundary conditions. Computations for three flow conditions are presented ($Kn_\infty = 0.032$, 0.011, and 0.001) with emphasis on results for the blunted cone-sting/afterbody configuration.

Computational Methods and Boundary Conditions

Both the molecular and continuum methods used are briefly described for the present application. The methods and requirements for application have been presented in previous publications in detail. Freestream conditions for the three cases examined are included in Table 1. The model configuration is shown in Fig. 1.

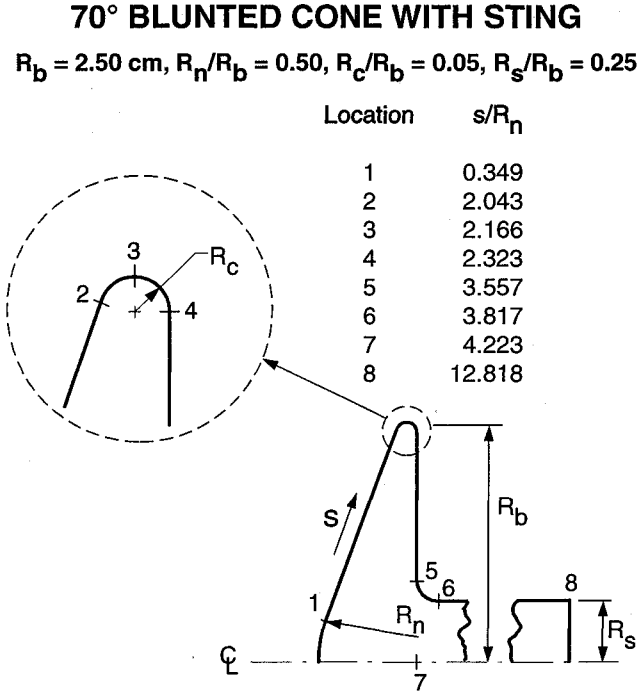

Fig. 1 Model configuration (base-sting fillet radius = 0.083 R_b).

Table 1 Conditions used in simulations[a]

Case	$\rho_\infty x10^5$, kg/m^3	V_∞, m/s	T_∞, K	M_∞	Kn_∞	Re_∞	Re_2
1	1.73	1502	13.3	20.2	0.032	768	28
2	5.19	1502	14.0	19.7	0.011	2,221	84
3	46.67	1633	15.0	20.6	0.001	20,610	726

[a]Uniform freestream conditions with nitrogen gas in thermal equilibrium at the freestream temperature. Model temperature equals 300 K. Diffuse surface with full thermal accommodation. The characteristic length is taken as the base diamter (0.05m).

Molecular Method

The direct simulation Monte Carlo (DSMC) method[5-7] provides a numerical capability that acknowledges the discrete nature of a gas and thereby provides a capability of simulating flows across the complete flow spectrum of continuum to free molecular flows. However, the DSMC method is normally applied to the transitional and free molecular flow regimes because the computing requirements can become excessive for continuum applications.

The computational domain is large enough so that the upstream and side boundaries can be specified as freestream conditions. The flow at the downstream outflow boundary is supersonic and vacuum conditions are specified. The outflow boundary was located 2.5 body diameters (0.125 m) downstream of the forebody stagnation point. Figure 1 presents information concerning model configuration. The computational domain is subdivided into several (either 13 or 14) unstructured regions with each region subdivided into computational cells (6–30,000). The number of simulated molecules is of the order of 20 per cell. Within a given region, each simulated molecule represents a fixed number of physical or real molecules (a large number of the order of 1.0×10^{10}). The unstructured regions allow one to substantially reduce the number of simulated molecules in the flow domain and still meet the basic numerical requirements of steady flow problems.

The molecular collisions are simulated using the variable hard sphere (VHS) molecular model. This model employs the simple hard sphere angular scattering law so that all directions are equally possible for postcollision velocity in the center-of-mass frame of reference. However, the collision cross section is a function of the relative energy in the collision. The freestream viscosity and mean free path are evaluated using the VHS collision model with $T_{ref} = 300$ K, $d_{ref} = 4.07 \times 10^{-10}$ m and $\bar{s} = 0.75$ (d_{ref} is the molecular diameter at reference temperature T_{ref} and $\bar{s}$ is the temperature exponent of the coefficient for viscosity). The freestream mean free path is calculated from the relation (see Ref. 5).

$$\lambda_\infty = \frac{(T_\infty/T_{ref})^\omega}{[\sqrt{2}n_\infty\sigma_{ref}(2-\omega)^\omega\Gamma(2-\omega)]} \quad (1)$$

$$\omega = \bar{s} - \tfrac{1}{2} \quad (2)$$

Energy exchange between kinetic and internal modes is controlled by the Larsen-Borgnakke[16] statistical model. For the present study, simulations are performed using a nonreacting gas model with one chemical species (N_2) while considering energy exchange between translational, rotational, and vibrational modes (rotational relaxation collision number of 5 and vibrational relaxation collision number of 50).

The effect of grid resolution on computed results is of particular interest for the present study. The results of such a study are included in Appendix A of Ref. 17 and results of futher grid refinement are included herein for Case 3.

Continuum Model

The Langley aerothermodynamic upwind relaxation algorithm (LAURA) of Gnoffo et al.[3] and Gnoffo[4] is used to provide the continuum flowfield solution. LAURA is an upwind-biased, point-implicit relaxation algorithm for obtaining the numerical solution to the governing equations for three-dimensional, viscous, hypersonic flows in thermochemical states ranging from perfect gas to both thermal and chemical nonequilibrium. For the results presented herein, however, only perfect gas solutions about axisymmetric geometries are included. A constant γ of 1.4 and a molecular weight of 28.0 is used to simulate the nonreacting nitrogen flow.

The LAURA tool has the capability to simulate the flowfield in the near wake region behind blunt bodies[2] in either a strongly coupled manner in which the forebody and the wake are computed simultaneously, or in an uncoupled manner in which the exit plane of the forebody solution is fixed as the inflow boundary condition for the wake calculation. The uncoupled approach requires less computational effort. The results presented in this paper are computed in the fully coupled manner. Viscosities are computed by Sutherland's Law[18] for nitrogen.

$$\mu = \frac{c_1 T^{3/2}}{(c_2 + T)} \tag{3}$$

For T in K and μ in Pa · s, $c_1 = 1.399 \times 10^{-6}$ and $c_2 = 106.7$. Thermal conductivities are defined by assuming a constant Prandtl number of 0.71.

A single-block volume grid with 120 cells along the solid surface and 84 cells normal to the surface is utilized for each of the cases. For all computations, the outflow boundary was located 0.115 m downstream of the forebody stagnation point. Orthogonality is true at the surface and cell Reynolds numbers at the wall are at most 3.0 (0.1 or less along the forebody). The grid is aligned to the bow shock for each case by first computing a preliminary solution on a three-block grid, then using that solution to assist the construction of the single-block grid. A 120×84 grid is judged as adequate based on past experiences with similar geometries.[2] The sensitivity of the calculated results to grid resolution is discussed in Ref. 17.

As the flow becomes more rarefied, the assumption of a continuum flow becomes tenuous and the conventional viscous flow no-slip conditions begin to fail. That is, the flow velocity at the surface takes a finite value (velocity slip) and the gas temperature at the surface differs from the surface temperature (temperature slip or jump). At the onset of slip, the continuum methodology often utilized to simply modify the surface boundary conditions. For the present Navier-Stokes calculations with slip boundary conditions, the following relations[19,20] are used:

$$v_s = 0 \tag{4}$$

$$u_s = \sqrt{\frac{\pi}{2}} \left(\frac{2-\theta}{\theta}\right) \frac{\mu_s}{\sqrt{P_s \rho_s}} \left(\frac{\partial u}{\partial \eta}\right)_s \tag{5}$$

$$T_s = T_w + \frac{1}{3}\sqrt{\frac{\pi}{2}} \left(\frac{\gamma}{\gamma-1}\right)\left(\frac{2-\theta}{\theta}\right)\left(\frac{k}{C_p}\right)_s \frac{1}{\sqrt{P_s \rho_s}} \left(\frac{\partial T}{\partial \eta}\right)_s \tag{6}$$

$$P_s = P_w + \frac{4}{5\sqrt{2\pi}} \left(\frac{\gamma}{\gamma-1}\right)\left(\frac{2-\theta}{\theta}\right) \frac{1}{T_s} \sqrt{\frac{P_s}{\rho_s}} \left(\frac{k}{C_p}\right)_s \left(\frac{\partial T}{\partial \eta}\right)_s \tag{7}$$

$$\rho_s = \rho_w \sqrt{\frac{T_w}{T_s}} \tag{8}$$

Equations (4–8) provide a relationship between the surface quantities and those at the edge of the Knudsen layer (a layer which is on the order of one mean free path in thickness from the surface). The subscript w denotes conditions at the wall and s refers to the edge of the Knudsen layer. Here, v is the velocity normal to the wall in the direction of η, u is the tangential velocity, and θ is the accommodation coefficient.

Results and Discussions

The flow conditions considered are particularly interesting because the forebody flow ranges from continuum to transitional as the overall Knudsen number increases from 0.001 to 0.03. However, the near wake produced by the 70-deg blunted cone shows evidence of rarefaction for all three flow conditions. With the presence of an afterbody sting, a wake vortex is calculated for each of the three flow conditions (Table 1) with the size of the vortex increasing with decreasing freestream Knudsen number. Calculations have been made with and without (See Ref. 14) a sting afterbody, however attention is focused on data obtained with an afterbody sting as wind tunnel tests[15] are planned for the model configuration and flow conditions considered herein. For the proposed experiments, measurements will include aerodynamics, surface heating rates, and near wake density mappings (electron beam fluorescence technique for cases 1 and 2). The sting length for the proposed experiments is 0.075 m. For the calculations, the sting is longer in that it extends to the end of the computational domain (lengths of 0.115 m and 0.105 m for the DSMC and Navier-Stokes calculations, respectively).

The DSMC method provides a capability of simulating flows across the spectrum of continuum to free molecular; being the benchmark method for simulating flows where transitional effects are important. This capability has been demonstrated by comparison with numerous experimental data sets. Two comparisons relevant to the current study are those of Refs. 10 and 21. In Ref. 10, comparisons are made with experimental data concerning the flow structure along the wake centerline produced by a sphere for Mach 5.6 flow at a $Kn_\infty = 0.005$. The comparisons made in Ref. 21 are for forebody and afterbody heating rates obtained in a vacuum chamber facility (Mach 7 for Kn_∞ of 0.057–0.178) for a candidate Venus aerobraking spacecraft. The vacuum chamber tests were for conditions where the flow was more rarefied and the heating rates lower (more than an order of magnitude lower) than that for the current study. Comparisons of the DSMC results with measured flow structure[10] and afterbody heating[21] are shown to be favorable. Consequently, the effects of rarefaction on surface quantities and flowfield structure are first demonstrated using the DSMC calculations as shown in Figs. 2–7. This is then followed by comparison of the DSMC and Navier-Stokes results.

Effects of Rarefaction as Calculated with Discrete Simulation Monte Carlo

The effects of rarefaction on the forebody flow structure are clearly evident from Fig. 2 where the density profiles along the stagnation streamline are presented for three flow conditions. For cases 1 and 2 ($Kn_\infty = 0.03$ and 0.01, respectively),

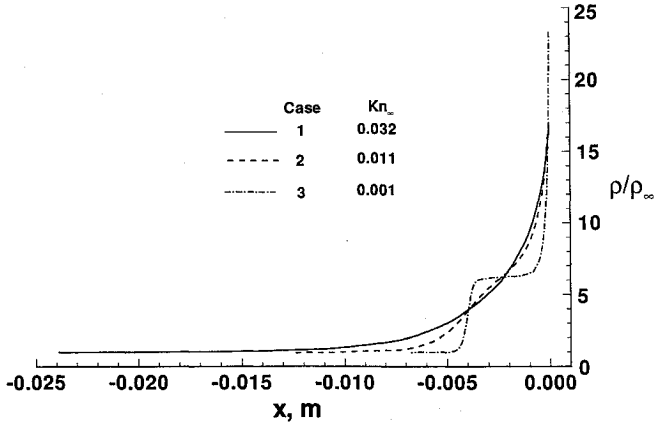

Fig. 2 Effect of rarefaction on stagnation streamline density profiles.

the density profiles show that the shock is very diffuse. However, for case 3 where $Kn_\infty = 0.001$, the density profile shows a distinct yet thick shock. Near the stagnation point, a substantial density increase occurs. This is characteristic of hypersonic flows about cold blunt surfaces.

Within the near wake, a stable vortex is calculated for each of the three flow conditions provided there is a sting afterbody. Without the sting, a distinct vortex is evident only for cases 2 and 3. The size of the vortex, Δ/d, is shown (Fig. 3) to increase exponentially with decreasing Kn_∞. The magnitude of Δ is the distance measured from the base plane to the wake stagnation point (the point in the wake where the separated flow reattaches and the velocity is zero).

For the present flow conditions, the calculated locations of reattachment (wake stagnation point) and peak heating on the sting differ substantially. Note that the maximum heating (Figs. 4 and 5) values along the sting do not occur as a sudden spike, but exist over an appreciable spatial extent that develops asymptotically. In the present results, there is a substantial difference between the wake stagnation and peak heating locations (Fig. 5), and this difference increases with increasing Kn_∞.

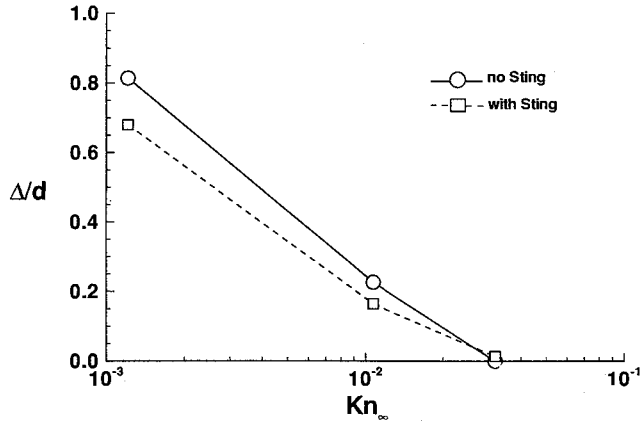

Fig. 3 Vortex size as a function of Knudsen number.

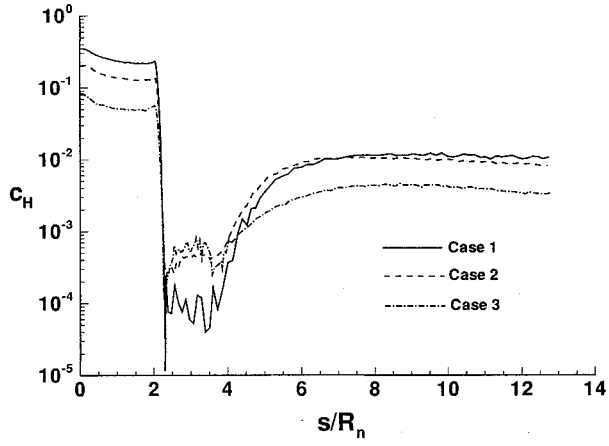

Fig. 4 Effect of rarefaction on surface heat transfer coefficients.

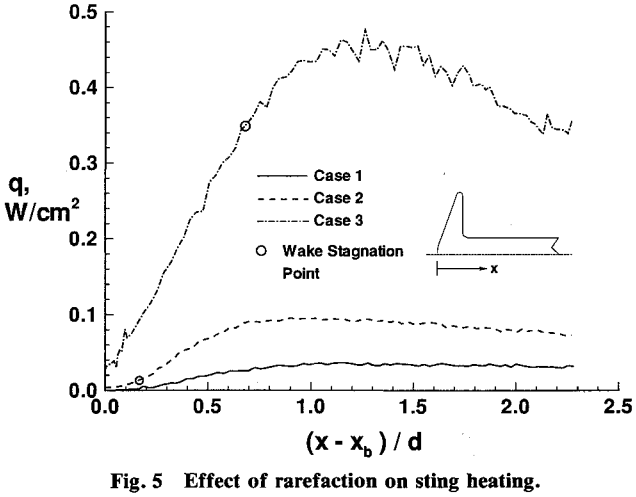

Fig. 5 Effect of rarefaction on sting heating.

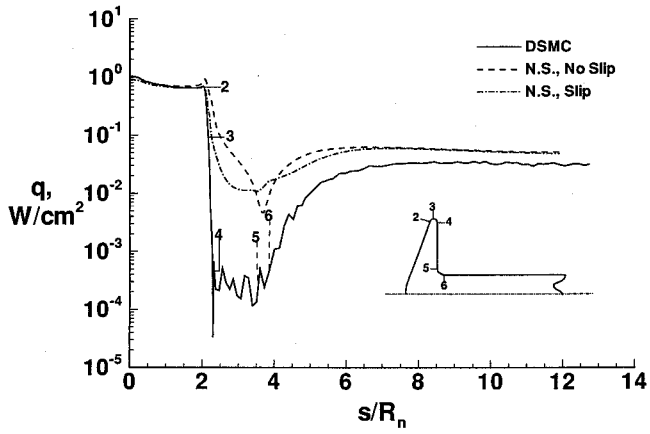

Fig. 6 DSMC and Navier-Stokes heating rate distributions (case 1).

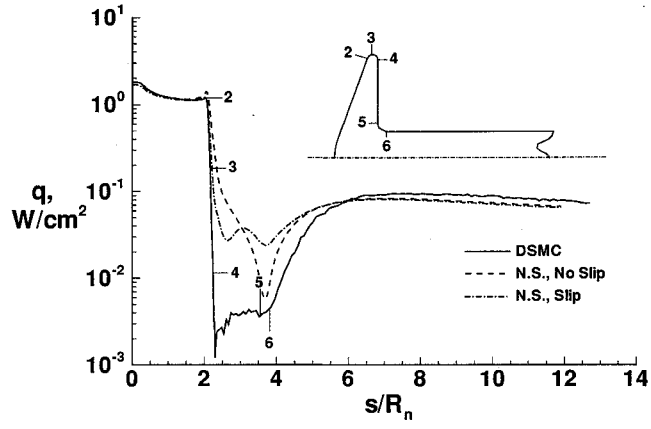

Fig. 7 DSMC and Navier-Stokes heating rate distributions (case 2).

The current findings are consistent with those reported by Brewer[10] where DSMC simulations were made for a 1.0-m-diam hemisphere with a 0.5-m cylindrical payload/afterbody. These calculations were for reacting air at the following conditions: freestream velocity of 10 km/s and altitudes of 86–110 km where the corresponding freestream Knudsen numbers ranged from 0.01 to 0.65. Results of these calculations show that the wake stagnation point on the payload was quite close to the aerobrake base plane, and the location of peak payload heating was further downstream of the aerobrake. Consequently, the DSMC results for both wind tunnel and flight conditions show that the heating rate along a sting/payload can be quite benign at the wake stagnation point provided the wake flow is in the transitional/rarefied regime. As the Knudsen number decreases, the heating rate at the wake stagnation point location approaches the peak heating value along the sting.

The maximum sting heating rates (Table 2) nondimensionalized by the forebody stagnation point value increase with decreasing Knudsen number. For case 1, the ratio is 0.036 while that for case 3 is 0.057. This trend is even more apparent along the base plane where (approximate values at $y/R_b = 0.5$) the nondimensional heating rate is 0.0003 for case 1 and 0.008 for case 3.

The surface heat transfer coefficients are presented in Fig. 4 for the three flow conditions. The heat transfer coefficients

Table 2 Direct simulation Monte Carlo results for blunted cone/sting configuration

	Drag			Heating Rate		
				Forebody stagnation point		
Case	Force, N	C_D	Percent due to friction	q, W/cm^2	C_H	Max. to sting, q, W/cm^2
1	0.064	1.68	8.4	1.0	0.349	0.036
2	0.183	1.59	5.9	1.8	0.202	0.095
3	1.905	1.56	2.0	8.4	0.083	0.476

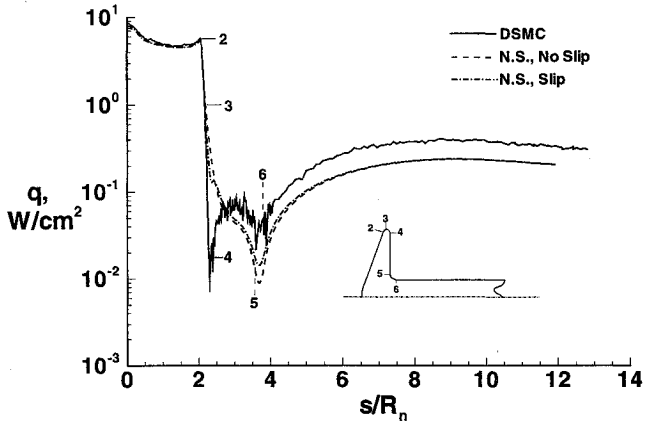

Fig. 8 DSMC and Navier-Stokes heating rate distributions (case 3).

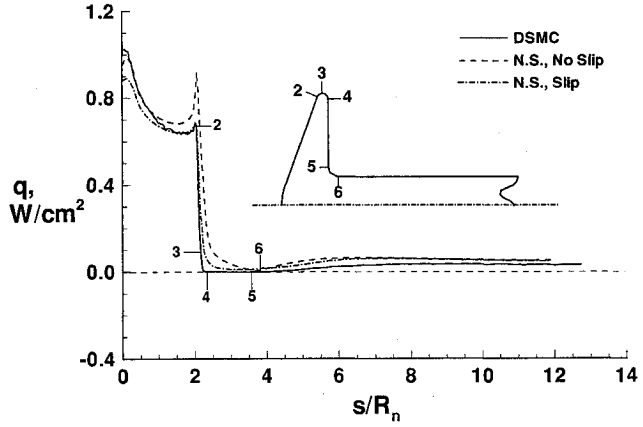

Fig. 9 DSMC and Navier-Stokes heating rate distributions (case 1).

are very sensitive to rarefaction effects. For the pressure coefficient, the data show (Ref. 17) a significant sensitivity only along the base plane and sting. These data show that the heat transfer coefficient along the forebody and sting, in general, experiences the same trend in that the fraction of freestream energy $C_H = 2q/\rho_\infty V_\infty^3$ transferred to the surface increases with increasing rarefaction. The reverse situation occurs along the base plane. In terms of aerodynamics, the drag coefficient (C_D = 1.68, 1.59, and 1.56 for cases 1-3, respectively) increases with rarefaction. Most of this increase is due to skin friction. The results show that the drag contribution due to friction increases from 2% for case 3 to 8.4% for case 1.

Comparison of Direct Simulation Monte Carlo and Navier-Stokes Results

Figures 6-9 present surface heating rate distributions (see Ref. 17 for surface pressure results) obtained with DSMC and LAURA calculations. LAURA results with and without slip are included. Figures 10-14 present flowfield data contrasting the DSMC and LAURA results.

Surface Results

The surface heating rates (Figs. 6-9) are presented as a function of nondimensional distance (s/R_n) along the surface measured from the stagnation point. The flow expansion about the base corner produces orders of magnitude reductions in surface quantities with respect to their forebody values. The semilog plots (Figs. 6-8) give a better perspective of the magnitude of heating along the base plane and sting. The DSMC results show a significant amount of scatter for part of the corner and base plane surface areas because of the very small sample size in these areas (see Ref. 22 for a more detailed discussion of this issue, which was most acute for case 1). Consequently, the DSMC surface data along the base plane are of use in establishing trends but not specific quantitative numbers. For case 1, the agreement for heating (Fig. 6) and pressure (Ref. 17) is poor along the base plane and sting. The

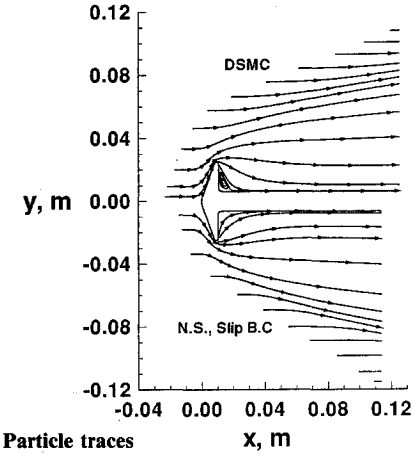

a) Particle traces

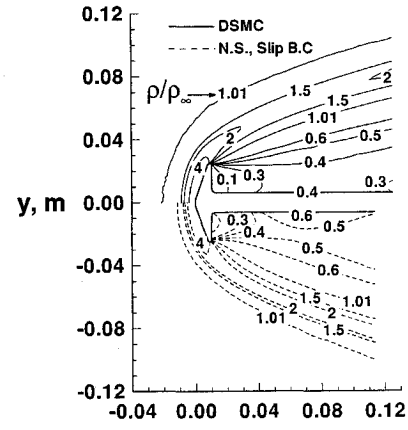

b) Density

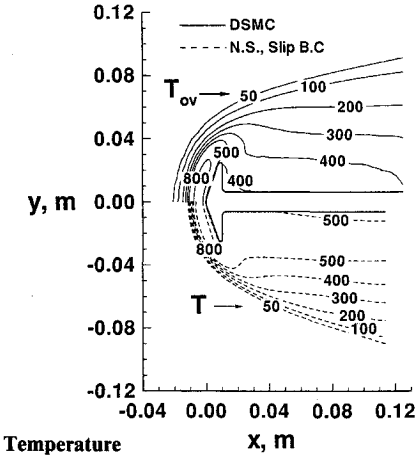

c) Temperature

Fig. 10 DSMC and Navier-Stokes flowfield values for case 1.

heating rates calculated with LAURA are more than an order of magnitude greater than the DSMC results. Along the sting, the LAURA results are high relative to the DSMC values [at an s/R_n value of 8 ($x = 0.065$ m), the LAURA results are a factor of two greater than the DSMC results]. The same general trends are evident for the surface pressure distributions (Ref. 17). With slip boundary conditions, the LAURA results are in closer agreement with the DSMC results, particularly along the base plane.

For case 2 (Fig. 7), the agreement between DSMC and LAURA are better, particularly along the sting where the LAURA heating rate value at $s/R_n = 8$ is 13% lower than the DSMC value. For case 3 (Fig. 8), the agreement along the base plane is the best for the three cases. Along the sting, the DSMC heating rates are substantially higher (at an s/R_n location of 8, the LAURA heating rate value is 45% lower than the DSMC value) than the LAURA values. For case 3, the LAURA results are essentially the same with or without slip.

A few overall comments are appropriate concerning the base plane and sting surface results. Inclusion of slip boundary conditions in the LAURA calculations had a very noticeable impact on the results along the base plane. Along the sting, the impact is confined to the near base region. Along the base plane, the agreement between DSMC and LAURA increased with decreasing Kn_∞ as would be expected. The same trend (agreement increasing with decreasing Kn_∞) for the sting was anticipated, but does not occur. The fact that the heating predictions differ by almost a factor of two along the sting for case 3 should be explored in more depth. Based on the grid resolution study reported in Ref. 17 and a subsequent DSMC grid refinement for case 3 (twice the number of cells used in Ref. 17 with the heating results shown in Fig. 8), it is

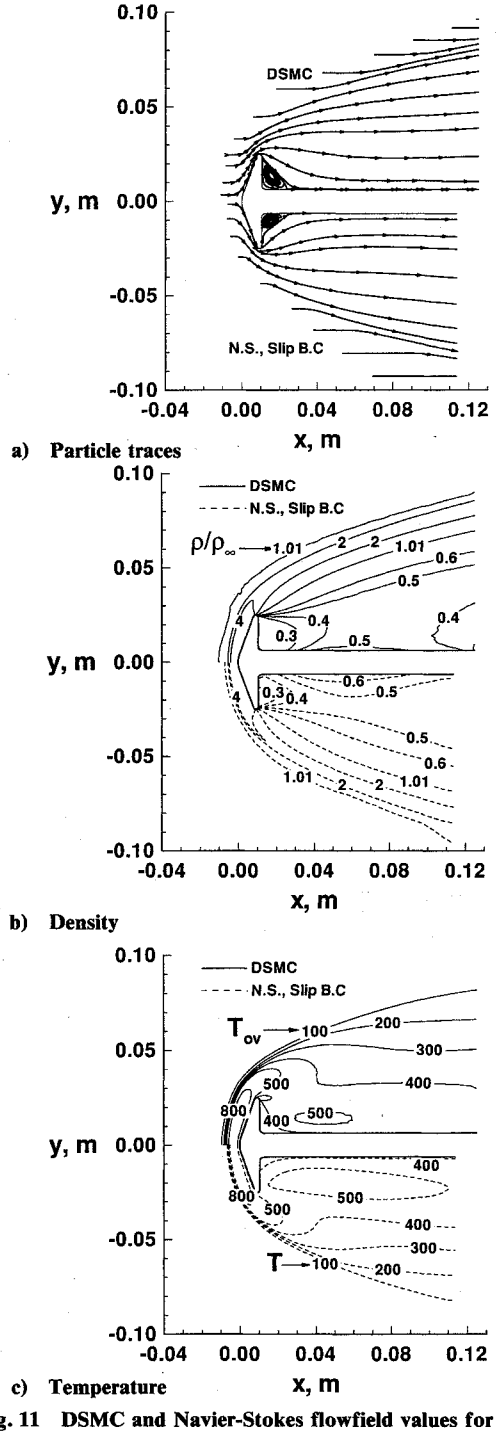

a) Particle traces
b) Density
c) Temperature

Fig. 11 DSMC and Navier-Stokes flowfield values for case 2.

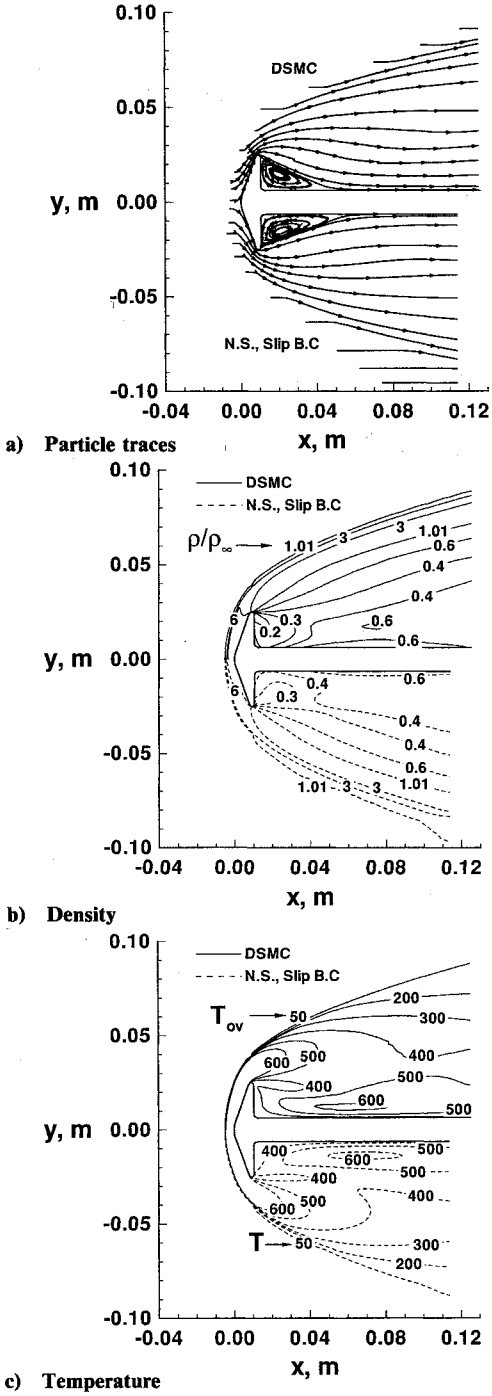

a) Particle traces
b) Density
c) Temperature

Fig. 12 DSMC and Navier-Stokes flowfield values for case 3.

concluded that the difference in heating rates along the sting cannot be explained in terms of grid resolution.

Along the forebody, the DSMC and LAURA results are in much closer agreement with the DSMC results for both heating rate and pressure being equal to or greater than the LAURA results. Figure 9 presents the heating rate distributions for case 1 in a format so that the forebody results are more clearly discernible. The maximum difference in heating is 13% (stagnation point) with slip. However, the no slip results are 30% higher than the DSMC values near the beginning of the corner expansion where the velocity and temperature jump are significant.

The forebody heating comparisons for case 2 (not shown) are in closer agreement with maximum differences of about 6% for the LAURA calculations with slip boundary conditions. For case 3, the agreement is 10% or better. The slip and no-slip calculations yield essentially the same results for case 3. A general statement concerning the forebody heating is that the heating predicted by DSMC is equal to or greater than the LAURA results with slip boundary conditions, and the maximum difference is less than 13% for all cases.

Comparisons of sting pressure distributions (presented in Ref. 17) show that the agreement between the two methods increases with decreasing rarefaction. (At $s/R_n = 8$, the LAURA results were a factor of two higher than the DSMC results for case 1 and 20% lower for case 3.) The same trends are evident for the pressure comparisons along the base. Also, as the rarefaction decreases, the agreement between the two methods improves for the minimum surface pressure location. For the DSMC results, this location was approximately the same for all cases, occurring just before the flow expands onto the base plane ($y = 0.024$ m). The DSMC results show that this location is where the flow separates as is evidenced by the surface shear stress. The LAURA calculations with or without slip boundary conditions show that the location of separation is delayed with respect to the DSMC values. LAURA results with slip show that the y locations for separation are 60 and 93% of the DSMC value for cases 2 and 3, respectively. The inclusion of slip delays separation and produces an earlier reattachment (smaller vortex).

Flow Structure

Comparisons of DSMC and LAURA results for flowfield structure are presented in Figs. 10–12 using contour plots. The contour comparisons are made for particle traces, density, and temperature. For case 1, (Fig. 10), the DSMC and LAURA comparisons exhibit a noticeable difference in flow structure: a small vortex with the DSMC calculation and none with LAURA, lower wake flowfield densities with DSMC, and a lower wake temperature with DSMC. The temperature comparisons are based on an overall kinetic temperature T_{ov} for the DSMC results (defined for a nonequilibrium gas as the weighted mean of the translational and internal temperature) and a thermodynamic temperature for the LAURA results. This particular comparison is not meaningful because the ideal gas equation of state does not apply[5] to T_{ov} in a nonequilibrium situation as is the situation for case 1. The thermodynamic temperature T is essentially an equilibrium gas property.

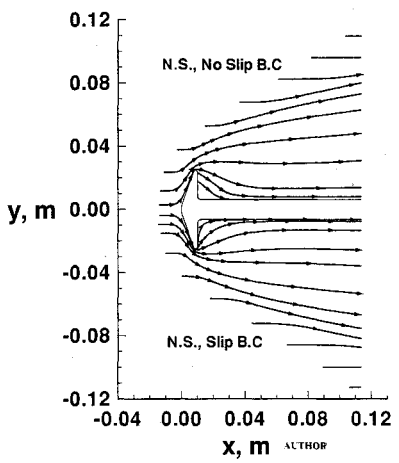

Fig. 13 Effect of slip boundary conditions on flow structure (case 1).

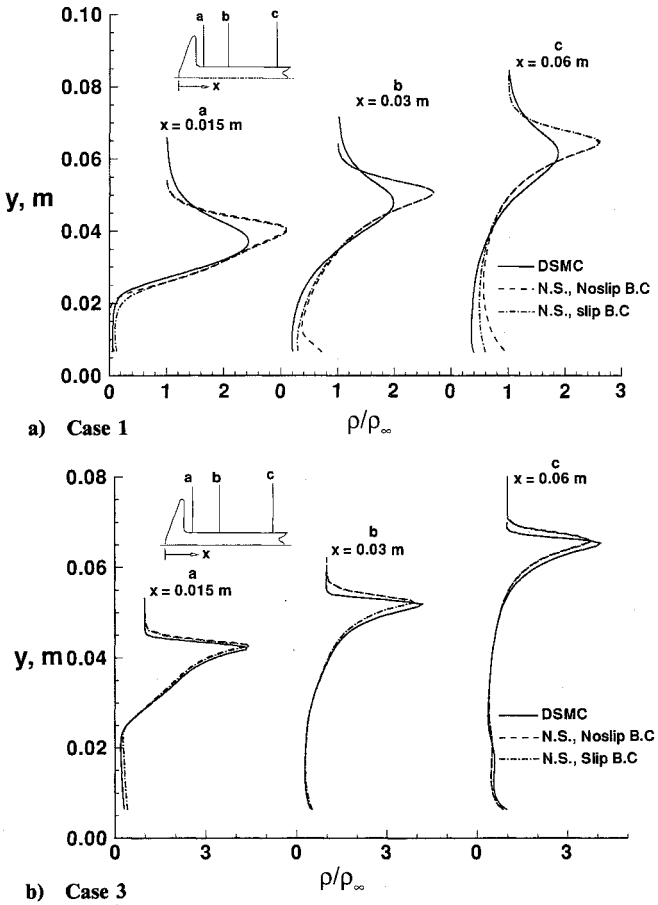

Fig. 14 DSMC and Navier-Stokes results for radial density profiles.

The particle traces in the near wake for case 1 (Fig. 13) appear to originate at the base plane surface when the LAURA calculation is made without slip boundary conditions. The same behavior was observed in Ref. 13 where a different Navier-Stokes program was applied to the problem of a monatomic gas flowing about a 70-deg blunted wedge. With slip boundary conditions, the particle traces have a more realistic behavior near the base plane.

As the Knudsen number decreases, the agreement between the two methodologies improves. For case 3, the general features of the flowfield are in good agreement.

Figures 14 present comparisons of DSMC and LAURA radial profiles at three axial locations in the wake for density. Data are presented for case 1 (Fig. 14a) and case 3 (Fig. 14b). LAURA solutions with and without slip are included. With slip boundary conditions, the LAURA results for case 1 are in better agreement with the DSMC results. For case 3, profiles for the two methodologies are in much better agreement, and the influence of slip boundary conditions on flowfield structure is negligible.

Concluding Remarks

Numerical solutions have been obtained for a blunt axisymmetric configuration [generic aeroassist space transfer vehicles (ASTV)] characterizing both the forebody and wake flows. The configuration is one that has been considered for Mars missions such as the Mars environmental survey (MESUR) network mission and the MESUR Pathfinder mission. The present study focused on specific wind tunnel conditions for

which an experiment is planned. Future opportunities will exist for direct comparison with experimental data.

Three freestream flow conditions are investigated (Knudsen numbers of 0.03, 0.01, and 0.001). The freestream was Nitrogen at Mach-20 conditions. The smaller Knudsen number case would normally be considered as continuum flow along blunt forebodies. The present results show that rarefaction effects are very evident as the flow expands into the near wake even for case 3 ($Kn_\infty = 0.001$). What is clear from the present calculations and those of Ref. 10 is that for both wind tunnel and flight conditions, the location of the wake stagnation and the location of the maximum convective heating rate along a sting/afterbody is not coincident. Furthermore, the separation between the two locations is a function of rarefaction. For wake flows, the convective heating rates near reattachment can be quite benign—only a small fraction of the peak sting/afterbody heating rate.

Both DSMC and Navier-Stokes methodologies have been applied to the current problem. The Navier-Stokes solutions were obtained with the LAURA code, both with and without slip boundary conditions. In general, the inclusion of slip boundary conditions provided improved agreement with the DSMC results. The findings of the present study differ from those of Ref. 13, where it is suggested that the Navier-Stokes equations can be employed for Knudsen numbers up to 0.05. The current study shows substantial differences in flowfield structure and surface results at a Knudsen number of 0.03. As the density of the freestream flow was increased (decreasing Knudsen number), the agreement between the two methodologies improved. For the smallest Knudsen number case (0.001), the overall agreement between the two methodologies is good with the exception of the heating rate to the sting where differences as large as a factor of two are observed.

References

[1]Anon., *America at the Threshold,* Report on the Synthesis Group on America's Space Exploration Initiative, Superintendent of Documents, U.S. Government Printing Office, Washington, DC, 1991, p. 59.

[2]Gnoffo, P. A., Price, J. M., and Braun, R. D., "Computation of Near-Wake, Aerobrake Flowfield," *Journal of Spacecraft and Rockets,* Vol. 29, No. 2, 1992, pp. 182–189.

[3]Gnoffo, P. A., Gupta, R. N., and Shinn, J. L., "Conservation Equations and Physical Models for Hypersonic Air Flows in Thermal and Chemical Nonequilibrium," NASA TP-2867, Feb. 1989.

[4]Gnoffo, P. A., "An Upwind-Biased, Point-Implicit Relaxation Algorithm for Viscous, Compressible Perfect-Gas Flows," NASA TP-2953, Feb. 1990.

[5]Bird, G. A., *Molecular Gas Dynamics,* Clarendon, Oxford, England, UK, 1976.

[6]Bird, G. A., "Monte Carlo Simulation in an Engineering Context," *Rarefied Gas Dynamics, Part 1,* edited by Sam S. Fisher, Vol. 74, Progress in Aeronautics and Astronautics, AIAA, New York, 1981, pp. 239–255.

[7]Bird, G. A., "Direct Simulation of Gas Flows at the Molecular Level," *Communications in Applied Numerical Method,* Vol. 4, 1988, pp. 165–172.

[8]Moss, J. N., and Price, J. N., "Direct Simulation of AFE Forebody and Wake Flow with Thermal Radiation," *Rarefied Gas Dynamics,* edited by E. P. Muntz, D. P. Weaver, and D. H. Campbell, Vol. 118, Progress in Aeronautics and Astronautics, AIAA New York, 1989, pp. 3413–3431.

[9]Celenligil, M. C., Moss, J. N., and Blanchard, R. C., "Three-Dimensional Rarefied Flow Simulations for the Aeroassist Flight Experiment Vehicle," *AIAA Journal,* Vol. 29, No. 1, 1991, pp. 52–57.

[10]Brewer, E. B., "Hypersonic Rarefied Wake Characterization," NASA TP-3327, Jan. 1993.

[11]Dogra, V. K., Moss, J. N., Wilmoth, R. G., and Price, J. M., "Hypersonic Rarefied Flow Past Spheres Including Wake Structure," AIAA Paper 92-0495, Jan. 1992.

[12]Dogra, V. K., Moss, J. N., and Price, J. M., "Near Wake Structure for a Generic ASTV Configuration," AIAA Paper 93-0271, Jan. 1993.

[13]Lumpkin, F. E., Boyd, I. D., and Venkatapathy, E., "Comparison of Continuum and Particle Simulations of Expanding Rarefied Flows," AIAA Paper 93-0728, Jan. 1993.

[14]Wilmoth, R. G., Mitcheltree, R. A., Moss, J. N., and Dogra, V. K., "Zonally-Decoupled DSMC Solutions of Hypersonic Blunt Body Wake Flows," AIAA Paper 93-2808, July 1993.

[15]Allegre, J., "The SR3 Low-Density Wind-Tunnel: Facility Capabilities and Research Development," AIAA Paper 92-3972, July 1992.

[16]Borgnakke, C., and Larsen, P. S., "Statistical Collision Model for Monte Carlo Simulation of Polyatomic Gas Mixture," *Journal of Computational Physics,* Vol. 18, No. 4, 1975, pp. 405–420.

[17]Moss, J. N., Mitcheltree, R. A., Dogra, V. K., and Wilmoth, R. G., "Hypersonic Blunt Body Wake Computations Using DSMC and Navier-Stokes Solvers," AIAA Paper 93-2807, July 1993.

[18]White, F. M., *Viscous Fluid Flow,* McGraw-Hill, New York, 1974.

[19]Davis, R. T., "Hypersonic Flow of a Chemically Reacting Binary Mixture Past a Blunt Body," AIAA Paper No. 70-805, June 1970.

[20]Gupta, R. N., Scott, C. D., and Moss, J. N., "Slip-Boundary Equations for Multicomponent Nonequilibrium Airflow," NASA TP-2452, Nov. 1985.

[21]Heyman, R. J., Schmitt, D. S., Alexander, S. G., and Bienkowski, G. K., "Base Heating on a Voir Aerobraking Configuration in Rarefied Flow," AIAA Paper 82-0877, June 1982.

[22]Moss, J. N., Dogra, V. K., and Wilmoth, R. G., "DSMC Simulations of Mach 20 Nitrogen Flows about a 70° Blunted Cone and its Wake," NASA TM 107762, Aug. 1992.